frontiers | Frontiers in Earth Science

TYPE Original Research
PUBLISHED 09 January 2023
DOI 10.3389/feart.2022.1100068

OPEN ACCESS

EDITED BY
Paolo Capuano,
University of Salerno, Italy

REVIEWED BY
Giovanni Martinelli,
National Institute of Geophysics and Volcanology, Section of Palermo, Italy
Gaetano De Luca,
Istituto Nazionale di Geofisica e Vulcanologia (INGV), Italy

*CORRESPONDENCE
Yang Xiang,
xiang_yangyang@yeah.net

SPECIALTY SECTION
This article was submitted to Solid Earth Geophysics, a section of the journal Frontiers in Earth Science

RECEIVED 16 November 2022
ACCEPTED 21 December 2022
PUBLISHED 09 January 2023

CITATION
Xiang Y and Peng S (2023), Hydrochemical and stable isotopes (δ^2H and δ^{18}O) changes of groundwater from a spring induced by local earthquakes, Northwest China. *Front. Earth Sci.* 10:1100068. doi: 10.3389/feart.2022.1100068

Hydrochemical and stable isotopes (δ^2H and δ^{18}O) changes of groundwater from a spring induced by local earthquakes, Northwest China

Yang Xiang[1,2]* and Suping Peng[1,2]

[1]China University of Mining & Technology (Beijing), Beijing, China, [2]State Key Laboratory of Coal Resources and Safe Mining, Beijing, China

It has been well reported that earthquakes can cause changes in groundwater chemistry and isotopes, and much of those changes were occurred in wells or hot springs; however, changes in cold spring caused by local small earthquakes have received less attention. Here, we collected continuous monitoring of the X10 spring (September 2018 to December 2019), investigated the hydrogeochemical characteristics of the spring by using water chemistry analysis and isotope methods. We compared the changes in water chemical ion concentrations and hydrogen-oxygen isotope ratios with the surrounding seismic activity, and the results show that 1) major chemical ion concentrations in X10 springs have an annual dynamic pattern of being high in winter and low in summer, and this change may be related to the seasonal effect of snowmelt; 2) the spring water originates from long-distant meteoric water, snowmelt, and bedrock fissure water and is affected by rock weathering and evaporation; 3) the hydrogen and oxygen stable isotope ratios and HCO_3^- concentration in groundwater are sensitive to local small seismic activity. We considered that small earthquakes can change the permeability in fault zones or aquifers, leading to mixing of groundwater with different chemical composition and isotopes. Our study demonstrates that the hydrogen and oxygen stable isotopes are more sensitive to seismic activity than the commonly used chemical constitutents, and that the sensitive constitutents vary in different observation wells or springs; therefore, combined monitoring of isotopes and water chemistry should be considered in the future to capture hydrogeochemical precursor signals caused by earthquakes.

KEYWORDS

X10 spring, stable isotopes, chemical components, seismic activity, permeability

1 Introduction

To identify possible earthquake precursor signals that could be effective in earthquake prediction and determination of impacts of earthquakes, various earthquake-related hydrological changes in water levels, temperatures, and stream flows have often been used as indicators (Wakita, 1975; King et al., 1995; Elkhoury et al., 2006; Wang and Manga, 2010; Shi et al., 2014; Manga and Wang, 2015; Wang and Manga, 2015; De Luca et al., 2018; Sun et al., 2018a; Sun et al., 2018b; Kim et al., 2019; Mastrorillo et al., 2020). However, groundwater hydrogeochemical changes, including changes in water chemical compositions and stable isotopes (δ^2H and δ^{18}O), may be more useful for a comprehensive and systematic

understanding of earthquake mechanisms (Thomas, 1988; Wakita, 1996; Woith et al., 2013; Ingebritsen and Manga, 2014; Manga and Wang, 2015). They have potential applications in identifying groundwater sources and tracking water chemical evolution (Capecchiacci et al., 2015; Cortes et al., 2016; Qi et al., 2017), and then revealing the groundwater circulation processes and its relationship with regional tectonic activity (Claesson et al., 2004; Claesson et al., 2007; Skelton et al., 2014; Mohr et al., 2017; Kim et al., 2020). Although changes in the major chemical ions and stable isotopes of hydrogen and oxygen in groundwater have been observed before and after earthquakes, the precursor signals that have been documented relatively rarely. This is due to the lack of continuous and long-term monitoring systems (Woith et al., 2013) and the fact that samples require expensive, time-consuming analysis in the laboratory. Therefore, the underlying mechanism of groundwater chemical changes caused by earthquakes remains unclear (Claesson et al., 2004; Claesson et al., 2007; Skelton et al., 2008; Reddy et al., 2011; Reddy and Nagabhushanam, 2012; Skelton et al., 2014; Barberio et al., 2017; Rosen et al., 2018; Li et al., 2019; Hosono and Masaki, 2020; Shi et al., 2020).

Groundwater usually originates from atmospheric precipitation, and its physical and chemical parameters are affected by crustal stress, surrounding rock properties, and deep fluids. In the process of earthquake generation and occurrence, regional tectonic stress alteration or local stress adjustments, subsurface rock micro-cracks evacuation, and deep and shallow fluid mixing can cause variations in the physicochemical properties or isotopes of groundwater in the fault zone and epicenter region (Du et al., 2008; Barberio et al., 2017; Chen and Wang, 2021). This can be attributed to earthquake-induced permeability changes in tectonic fault zones/aquifers, or rupture of hydraulic barriers in aquifers (Skelton et al., 2014; Shi et al., 2020). Thus, the groundwater in the fault zone, especially the springs, contains abundant information about crustal stress. Analyzing the hydrogeochemical characteristics of springs can help reveal the influence of tectonic activity on the groundwater system and capture the possible earthquake precursor signals (Thomas, 1988; Claesson et al., 2004; Claesson et al., 2007; Skelton et al., 2014; Wästeby et al., 2014; Wang and Manga., 2015; Barberio et al., 2017; Shi and Wang., 2017; Skelton et al., 2019; Chen and Wang, 2021; Yang et al., 2021).

Understanding the impact of tectonic activity on groundwater resources is important for earthquake hazard risk assessment in seismically active areas. In recent decades, studies on the characteristics of groundwater chemistry and hydrogen–oxygen stable isotopes before and after earthquakes have made remarkable progress and have obtained variations in hydrochemical signals related to earthquakes (Claesson et al., 2004; Wang et al., 2005; Claesson et al., 2007; Skelton et al., 2014; Onda et al., 2018; Skelton et al., 2019). For example, Na^+ and Cl^-concentrations in groundwater nearly doubled within 1 week in the Cokcapinar area after the 1998 Adana *M* 6.2 earthquake (Woith et al., 2013). Cl^-concentration in hot springs increased exponentially before the September 1999 Jiji earthquake in Taiwan (Song et al., 2005). Some hydrochemical ion concentrations and δ^2H and $\delta^{18}O$ significantly increased before the *M* 5.8 earthquake in the Tjörnes Fracture Zone in northern Iceland in September 2002 and decreased after the earthquake (Claesson et al., 2004). Na^+, Si, and Ca^{2+} concentrations and δ^2H and $\delta^{18}O$ in groundwater exhibited apparent high-value anomalies in the seismic region before and after the *M* 5.5 and *M* 5.6 earthquakes in Iceland in October 2012 and April 2013, respectively (Skelton et al., 2014). Several mechanism models have been proposed to explain the hydrogeochemical changes associated with earthquakes, such as increased solubility of rocks due to increased crustal stress and release of ions from rocks into water (Etiope et al., 1997), pore collapse due to fluid discharge (Inan et al., 2013), contact of water with exposed fresh rock surfaces, enhanced water–rock interaction (Du et al., 2010), groundwater mixing between different aquifers due to disruption of the aquifer hydraulic barrier (Wang et al., 2004), and tectonic compression leading to the uplift of deep fluids into shallow regional aquifers (Dadomo et al., 2013; Barberio et al., 2017). Among these mechanisms, the crustal strain dilation or aquifer permeability changes causing mixtures of different waters are usually considered to be the mechanism to explain these changes (Woith et al., 2013; Skelton et al., 2014).

The response of water chemistry components and hydrogen–oxygen stable isotopes to large earthquakes has been reported in wells or hot springs (Shi et al., 2014; King, 2018); however, changes in cold spring caused by local small earthquakes have received less attention. In the present study, the major chemical compositions and hydrogen–oxygen stable isotopes were continuously monitored by regular sampling (every 5 days) of the X10 spring (cool spring) on the Hongyanchi fault zone. This study aims to evaluate the potential of combining δ^2H and $\delta^{18}O$ ratios and water chemistry composition methods in groundwater to discriminate regional tectonic activity and thus provide evidence for earthquake risk assessment in tectonically active areas.

2 Geological setting and seismicity

The X10 spring is located south of Urumqi in the Xinjiang autonomous region of China at an altitude of 1088 m (Figure 1A). The spring is dynamic and stable with abundant water. The water temperature is stable at approximately 11.4°C all year round, and the water flow ranges from 2.0 to 7.0 L/s. In terms of geological structures, this spring is situated at the intersection of the Hongyanchi thrust fault and its subsidiary fault. The Hongyanchi fault is located in the depression at the southern edge of the Junggar Basin, at the western end of the Bogda Mountain tectonic zone, with the direction of NWW, extending for more than 30 km. The nature of the fault is left-lateral compression-torsion, and joint fractures and near-vertical weathering fractures are commonly developed in the original rock stratum on the two sides of the fault. The fractures are mainly filled with minerals of shallow origin, such as gypsum and kaolin. The spring gushes out along the fracture zone, and the exposed strata are Permian gray sand conglomerate and gray-black mudstone, with a small amount of gray-brown shale. According to the earthquake catalog of the China Earthquake Network center, a total of 37 earthquakes of *M* 3 or above occurred within a range of 150 km around the X10 spring between September 2018 and December 2019.29 earthquakes of intensity *M* 3.0–3.9, 7 earthquakes of *M* 4.0–4.9, and 1 earthquake of *M* 5 and above (Figure 1B).

3 Materials and methods

In this study, major chemical ions and hydrogen and oxygen stable isotope in the X10 spring water were continuously monitored from

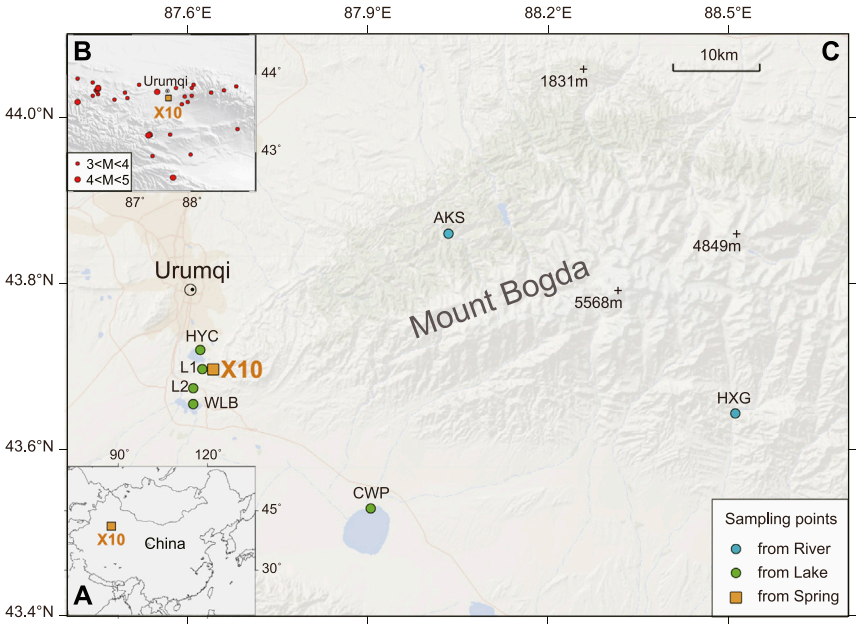

FIGURE 1
Overview of the study area. **(A)** Location of the monitored spring is displayed with a yellow square. **(B)** Red circles represent the epicenters of the main historical earthquakes that have occurred in the area. **(C)** The green and blue circles represent lake and river water sampling points, respectively.

TABLE 1 Hydrochemistry data for different water bodies.

Points	Water type	Na^+ mg/L	K^+ mg/L	Mg^{2+} mg/L	Ca^{2+} mg/L	Cl^-mg/L	SO_4^{2-}mg/L	NO_3^-mg/L	HCO_3^-+CO_3^{2-}mg/L	TDS mg/L	δ^2H ‰	$\delta^{18}O$ ‰
X10*	spring	379.87	2.76	55.14	58.96	272.32	501.31	3.58	295.71	1423.58	−89.06	−12.46
L1	Lake	442.06	3.42	77.54	97.68	290.17	673.40	2.09	260.16	1718.44	−86.20	−12.01
CWP	Lake	178.81	3.35	36.92	126.47	172.48	507.72	35.30	140.34	1131.86	−73.37	−9.97
AKS	River	2.27	0.22	1.57	15.41	2.12	14.61	5.27	48.81	65.99	−73.00	−11.29
HXG	River	6.17	0.35	4.70	30.14	5.49	26.26	6.80	103.73	131.90	−72.08	−10.99
L2	Lake	425.12	3.09	60.68	71.06	258.15	506.42	1.11	350.42	1501.71	—	—
WLB	Lake	30.17	1.11	8.56	53.64	30.43	122.09	5.39	103.73	303.53	—	—
HYC	Lake	99.50	2.86	16.44	70.21	61.89	214.78	4.86	127.43	534.92	—	—
	Rain										−64.93	−10.28
	Rain										−74.41	−10.46
	Snow										−120.65	−15.34
	Snow										−145.59	−17.71

X10* is the average value of continuous monitoring of X10 springs (n=94).

September 2018 to December 2019, with a sampling interval of 5 days at 10:00 a.m. on each sampling day. The results are shown in Table 1 and Table 2. A total of 94 groups of spring samples were collected. Eight samples of precipitation (rainfall and snowmelt) from the Urumqi area and surface water (river and lake) near the X10 spring were collected. All sampling locations are shown in Figure 1C. Samples for analyzing major ions concentrations and isotopes of hydrogen and oxygen were collected with 60-mL and 30-mL polyethylene bottles, respectively. Each sample was stored full in cleaned polyethylene bottles and filtered through a 0.45 μm membrane before measured. All water samples were examined in the Laboratory of Crustal Dynamics, China Earthquake Administration. Concentrations of HCO_3^- and CO_3^{2-} ions were determined using the traditional titration with HCl. Na^+, K^+, Ca^{2+}, Mg^{2+}, SO_4^{2-}, NO_3^- and Cl^- concentrations were measured using ICS-2100 ion chromatography. The reliability of chemical data was

TABLE 2 Concentrations of major chemical constituents in the X10 spring.

Date	Na^+ mg/L	K^+ mg/L	Mg^{2+} mg/L	Ca^{2+} mg/L	Cl^-mg/L	SO_4^{2-}mg/L	NO_3^-mg/L	HCO_3^-+CO_3^{2-}mg/L	TDS mg/L	δ^2H ‰	$\delta^{18}O$ ‰
20180915	451.14	3.08	64.98	75.85	262.26	505.77	2.45	302.64	1517.47	−89.22	−12.61
20180920	498.62	3.69	70.18	61.68	293.83	565.62	0.13	307.95	1648.65	−89.46	−12.54
20180925	501.20	3.51	70.63	75.32	294.10	567.71	0.14	318.57	1672.94	−89.04	−12.36
20180930	498.28	3.26	68.30	51.94	293.66	569.21	0.01	281.40	1626.37	−88.84	−12.37
20181005	478.44	3.37	68.22	64.91	294.98	568.10	0.02	318.57	1638.31	−89.62	−12.52
20181010	323.83	2.24	46.70	52.68	292.41	562.26	0.07	313.26	1437.71	−89.82	−12.69
20181015	482.19	3.21	68.30	58.21	293.67	562.00	0.06	313.26	1625.17	−89.22	−12.47
20181020	466.84	3.14	67.40	71.72	296.31	565.52	0.04	329.19	1636.46	−88.80	−12.31
20181025	441.09	2.73	64.40	78.04	284.77	541.65	1.58	323.13	1576.74	-89.31	−12.48
20181030	450.12	2.75	65.65	76.56	283.90	538.65	1.15	323.13	1581.22	−89.85	−12.76
20181104	446.64	2.72	65.22	76.33	282.99	533.09	1.26	323.13	1570.57	−89.35	−12.61
20181109	447.91	2.83	65.33	76.92	283.06	536.18	0.02	323.13	1574.59	−89.30	−12.56
20181114	451.75	2.85	65.65	76.25	286.13	537.01	0.02	323.13	1582.10	−89.43	−12.58
20181119	453.51	2.84	65.51	76.65	282.30	527.95	0.02	307.24	1563.35	−88.72	−12.30
20181124	454.26	2.85	65.57	75.89	286.60	532.72	0.03	317.83	1577.86	−89.85	−12.71
20181129	441.99	2.81	63.58	74.91	280.53	521.85	0.01	317.83	1545.38	−90.27	−12.71
20181204	262.94	0.96	38.29	44.81	264.68	509.17	5.89	322.14	1288.40	−90.17	−12.86
20181209	304.84	1.33	44.20	50.24	146.83	290.06	3.95	332.70	1009.19	−90.07	−12.88
20181214	314.41	1.43	45.26	51.03	259.23	497.45	6.10	322.14	1336.56	−89.58	−12.45
20181219	321.28	1.43	46.54	54.15	263.54	506.73	5.25	327.42	1363.25	−90.25	−13.00
20181224	339.95	1.75	48.66	52.18	265.05	507.49	5.67	327.42	1385.08	−89.81	−12.74
20181229	326.64	1.63	46.84	53.14	264.88	506.98	2.54	332.70	1369.74	−90.60	−13.00
20190103	361.12	2.15	54.11	61.87	261.17	476.72	1.50	311.19	1374.40	−88.23	−12.22
20190108	365.09	2.26	54.73	62.55	264.32	481.65	3.12	305.09	1386.44	−88.66	−12.41
20190113	365.10	2.21	54.58	61.56	264.17	481.63	1.68	292.88	1377.55	−87.92	−12.14
20190118	358.73	2.12	53.52	61.16	259.07	472.44	1.08	292.88	1354.69	−88.96	−12.36
20190123	362.78	2.18	54.14	61.24	253.94	463.47	1.29	286.78	1342.50	−89.01	−12.34
20190128	357.96	2.03	52.87	59.52	261.55	479.83	6.62	323.39	1382.35	−88.63	−12.31
20190202	361.52	2.35	53.35	59.88	262.37	481.49	5.14	298.98	1375.87	−88.85	−12.33
20190207	355.10	2.14	52.44	60.25	256.66	471.17	4.94	311.19	1358.51	−89.13	−12.35
20190212	362.78	2.16	53.28	59.00	259.48	475.61	4.69	311.19	1372.85	−88.93	−12.42
20190217	360.84	2.22	53.01	60.64	260.38	475.32	4.71	311.19	1373.06	−88.20	−12.18
20190222	353.58	2.33	52.29	58.27	257.66	472.30	5.37	305.09	1354.66	−88.60	−12.33
20190227	351.73	1.95	43.68	49.34	256.59	471.01	3.42	292.88	1324.41	−89.04	−12.50
20190304	354.33	2.35	51.45	57.89	258.98	474.60	3.41	305.09	1355.82	−88.71	−12.40
20190309	360.38	2.15	51.24	58.77	261.85	476.53	4.73	305.09	1368.47	−89.04	−12.54
20190314	358.97	2.15	51.88	58.08	257.39	472.16	0.01	317.29	1359.52	−89.50	−12.56
20190319	363.01	2.18	52.59	58.81	263.91	480.69	0.03	311.19	1377.11	−89.10	−12.42

(Continued on following page)

TABLE 2 (*Continued*) Concentrations of major chemical constituents in the X10 spring.

Date	Na^+ mg/L	K^+ mg/L	Mg^{2+} mg/L	Ca^{2+} mg/L	Cl^-mg/L	SO_4^{2-}mg/L	NO_3^-mg/L	HCO_3^-+CO_3^{2-}mg/L	TDS mg/L	δ^2H ‰	$\delta^{18}O$ ‰
20190324	363.19	2.22	52.33	59.03	263.73	479.10	0.02	317.29	1378.56	−89.05	−12.43
20190329	364.46	2.38	52.55	58.64	264.57	479.31	0.03	317.29	1380.91	−89.03	−12.40
20190403	315.25	1.89	43.53	49.76	254.03	473.43	5.79	311.19	1299.97	−88.25	−12.18
20190408	310.99	1.02	42.79	49.07	253.04	471.06	4.65	311.19	1288.92	−88.74	−12.38
20190413	314.70	1.25	42.85	48.06	254.87	473.36	7.06	298.98	1292.35	−88.75	−12.40
20190418	303.74	1.37	42.28	50.15	247.42	458.26	4.40	323.39	1269.94	−89.64	−12.64
20190423	304.21	1.42	42.22	50.11	247.19	457.84	3.22	305.09	1259.25	−89.40	−12.56
20190428	303.16	1.44	42.18	50.01	247.28	464.62	1.78	298.98	1260.68	−89.32	−12.61
20190503	302.92	1.43	42.04	49.83	248.32	465.71	1.95	305.09	1265.58	−89.20	−12.54
20190508	304.94	1.52	42.20	50.05	240.01	441.70	4.43	298.98	1234.95	−88.78	−12.44
20190513	304.02	1.51	42.16	50.15	238.84	444.06	1.06	305.09	1234.90	−89.02	−12.55
20190518	306.57	1.64	42.32	50.25	242.25	446.48	3.72	298.98	1243.35	−89.52	−12.42
20190523	304.74	1.48	42.03	49.97	243.41	448.71	1.39	305.09	1244.92	−88.74	−12.53
20190528	307.03	1.38	42.16	49.96	240.80	445.40	1.18	298.98	1238.03	−89.04	−12.58
20190602	327.94	2.20	46.50	55.15	254.78	477.97	2.60	305.09	1322.60	−89.23	−12.62
20190607	324.79	2.26	46.00	55.20	255.03	478.73	2.17	305.09	1319.66	−89.36	−12.65
20190612	326.91	2.18	46.40	55.89	254.30	474.67	0.12	292.88	1309.56	−89.54	−12.66
20190617	324.46	2.60	45.98	55.73	257.78	484.89	0.16	323.39	1335.98	−89.95	−12.92
20190622	332.18	2.38	46.81	55.22	258.02	478.62	0.14	317.29	1334.69	−89.66	−12.76
20190627	375.04	2.76	53.20	61.61	257.29	480.66	0.15	353.90	1410.30	−89.51	−12.73
20190705	387.99	3.48	54.46	66.19	271.26	478.27	5.42	292.88	1416.96	−87.87	−12.16
20190710	371.77	3.24	51.75	42.45	269.68	476.62	3.22	256.27	1350.19	−87.93	−12.06
20190715	314.25	2.90	43.82	45.71	269.03	479.02	5.92	268.47	1298.26	−88.03	−12.12
20190720	384.09	3.35	53.98	48.97	269.34	482.15	3.73	280.68	1389.24	−88.04	−12.19
20190725	387.74	3.36	55.13	48.73	270.10	487.86	3.19	244.07	1381.46	−88.41	−12.30
20190730	387.39	3.32	55.94	56.32	268.72	487.58	3.61	280.68	1406.54	−88.52	−12.32
20190805	401.57	4.52	57.35	54.08	275.56	495.65	10.54	244.07	1424.61	−89.02	−12.49
20190810	387.61	3.44	56.19	53.71	272.58	495.35	5.98	256.27	1406.27	−88.92	−12.62
20190815	297.87	2.69	43.08	40.54	276.17	502.12	4.87	274.58	1307.91	−88.50	−12.28
20190820	397.67	3.39	58.46	68.49	281.15	512.00	4.75	250.17	1454.34	−88.99	−12.31
20190825	395.07	3.36	58.12	51.82	281.14	508.51	3.11	274.58	1441.68	−88.73	−12.10
20190830	401.43	3.44	58.78	51.02	284.90	511.80	3.85	274.58	1455.78	−88.93	−12.14
20190905	406.85	3.50	60.02	53.97	288.09	518.57	3.88	268.47	1472.35	−88.66	−12.28
20190910	399.51	3.53	59.47	60.61	289.91	520.93	5.35	286.78	1486.01	−88.73	−12.41
20190915	407.64	3.58	60.37	56.45	293.94	526.42	5.55	268.47	1491.49	−88.86	−12.51
20190920	407.69	3.66	61.16	71.94	297.45	531.21	6.56	262.37	1514.25	−89.40	−12.86
20190925	411.48	3.67	61.34	59.11	299.11	536.70	5.75	256.27	1508.65	−89.14	−12.94
20190930	417.98	3.83	62.95	55.94	299.07	535.47	4.26	268.47	1517.03	−89.11	−13.04

(Continued on following page)

TABLE 2 (*Continued*) Concentrations of major chemical constituents in the X10 spring.

Date	Na^+ mg/L	K^+ mg/L	Mg^{2+} mg/L	Ca^{2+} mg/L	Cl^-mg/L	SO_4^{2-}mg/L	NO_3^-mg/L	HCO_3^-+CO_3^{2-}mg/L	TDS mg/L	δ^2H ‰	$\delta^{18}O$ ‰
20191005	413.51	4.19	62.20	59.70	301.10	538.95	5.38	292.88	1534.82	−89.21	−12.53
20191010	422.93	4.07	63.26	58.37	303.85	543.13	5.33	262.37	1535.44	−89.43	−12.45
20191015	427.75	4.18	64.47	61.99	291.70	524.21	5.85	268.47	1517.67	−89.39	−12.52
20191020	415.60	3.92	63.13	76.36	299.82	540.58	6.75	292.88	1555.96	−88.54	−12.10
20191025	410.17	3.93	62.06	59.86	298.32	539.70	6.82	274.58	1521.42	−88.97	−12.22
20191030	415.22	3.88	62.70	58.21	299.49	540.09	6.13	274.58	1526.28	−88.85	−12.10
20191105	422.94	4.09	62.81	59.40	305.01	548.20	5.44	268.47	1545.55	−89.52	−12.16
20191110	408.86	3.83	62.27	59.99	296.15	533.74	6.12	256.27	1502.37	−89.02	−12.17
20191115	415.77	3.84	62.52	62.09	301.83	541.65	5.90	244.07	1518.94	−89.46	−12.30
20191120	408.10	3.82	62.22	73.74	290.72	531.13	8.90	268.47	1516.20	−87.91	−12.19
20191125	416.12	3.90	62.53	60.39	289.33	524.07	6.68	262.37	1497.44	−88.30	−12.30
20191130	405.17	3.77	61.71	59.04	289.21	525.65	6.04	262.37	1485.02	−88.66	−12.29
20191205	402.54	3.73	60.96	59.88	288.10	521.17	7.42	286.78	1490.43	−88.84	−12.40
20191210	401.16	3.74	60.67	57.12	288.91	520.97	6.10	262.37	1473.08	−88.56	−12.27
20191215	416.63	3.67	62.82	83.09	300.64	541.31	7.04	262.37	1549.77	−88.95	−12.35
20191220	398.05	3.64	60.33	57.98	282.18	507.12	5.50	280.68	1458.29	−89.12	−12.41
20191225	405.60	3.76	61.04	59.45	287.88	515.97	5.89	274.58	1480.10	−89.16	−12.41
20191230	404.27	3.64	60.45	57.82	288.05	515.11	5.93	311.19	1494.11	−88.87	−12.42

checked by the charge balance errors. Calculated charge balance errors were less than ± 10% which is an acceptable uncertainty in this study. The δ^2H and $\delta^{18}O$ values were measured with a LWIA 912–0008 liquid water isotope analyzer from Los Gatos Research with an accuracy of 0.1‰ for $\delta^{18}O$ and an accuracy of 0.3‰ for δ^2H.

4 Results

4.1 Hydrochemical characteristics

4.1.1 Hydrochemical types

As shown in Table 2, the proportion of cation concentration in the X10 spring was Na^+>Ca^{2+}>Mg^{2+}>K^+, and the average values of each ion content were 379.87 mg/L, 58.96 mg/L, 55.14 mg/L, and 2.76 mg/L, respectively. The dominant cations were Na^+ and Ca^{2+}, and Na^+ concentration accounted for approximately 76% of the total cation concentration. The relationship of anion concentration was SO_4^{2-}>HCO_3^->Cl^->NO_3, and the average values of each ion content were 501.31 mg/L, 295.71 mg/L, 272.32 mg/L, and 3.58 mg/L, respectively. SO_4^{2-} and HCO_3^- predominated in the spring samples, and their combined concentration accounted for approximately 74% of the total anion concentration. The hydrochemistry type of the X10 spring is SO_4·Cl–Na. The content of total dissolved solids (TDS) ranged from 1.0 to 1.67 g/L, with an average of 1.42 g/L.

Analyzing the correlation between conventional ions in groundwater helps to understand the relationship between each component and the variation in their content. The Pearson correlation coefficients (r) were calculated for all components involved in the hydrochemistry of the X10 spring (Figure 2). The results showed that most ions exhibited acceptable linear trends with at least one other ion (Pearson's $r > 0.5$; $p < 0.05$). The strongest correlation was between Na^+ and Mg^{2+}, with a correlation coefficient of 0.96, followed by SO_4^{2-} and Cl^-, with a correlation coefficient of 0.92, indicating that the chemical composition of the X10 spring was stable. Cl^-correlated strongly with each cation (except Ca^{2+}), and SO_4^{2-} correlated strongly with Na^+ and Mg^{2+}. HCO_3^- was strongly correlated with K^+ only and showed a negative correlation ($r = -0.67$), whereas its correlation with other cations was weak or irrelevant, indicating that the change of HCO_3^- concentration may be affected by other factors.

4.1.2 Factor analysis of hydrochemical characteristics

The equivalence ratios of $Na^+/(Na^+ + Ca^{2+})$ and $Cl^-/(Cl^- + HCO_3^-)$ *versus* TDS were used to create the Gibbs diagrams. This method has been widely used to identify the effects of rock weathering, precipitation, and evaporation on water chemistry (Gibbs, 1970). HXG and AKS river samples that have $Na^+/(Na^+ + Ca^{2+})$ or $Cl^-/(Cl^- + HCO_3^-)$ ratios less than 0.5 and are distributed in the interface region of rock weathering and precipitation (Figure 3). Other samples (CWP, L1, L2, HYC, WLB, and X10 spring), most of which are distributed in the evaporative and rock-weathering dominance area, have $Na^+/(Na^+ + Ca^{2+})$ (Figure 3A) or $Cl^-/(Cl^- + HCO_3^-)$ (Figure 3B) ratios ranging from 0.5 to 1. The distributed feature of samples shows that evaporative and rock weathering are the

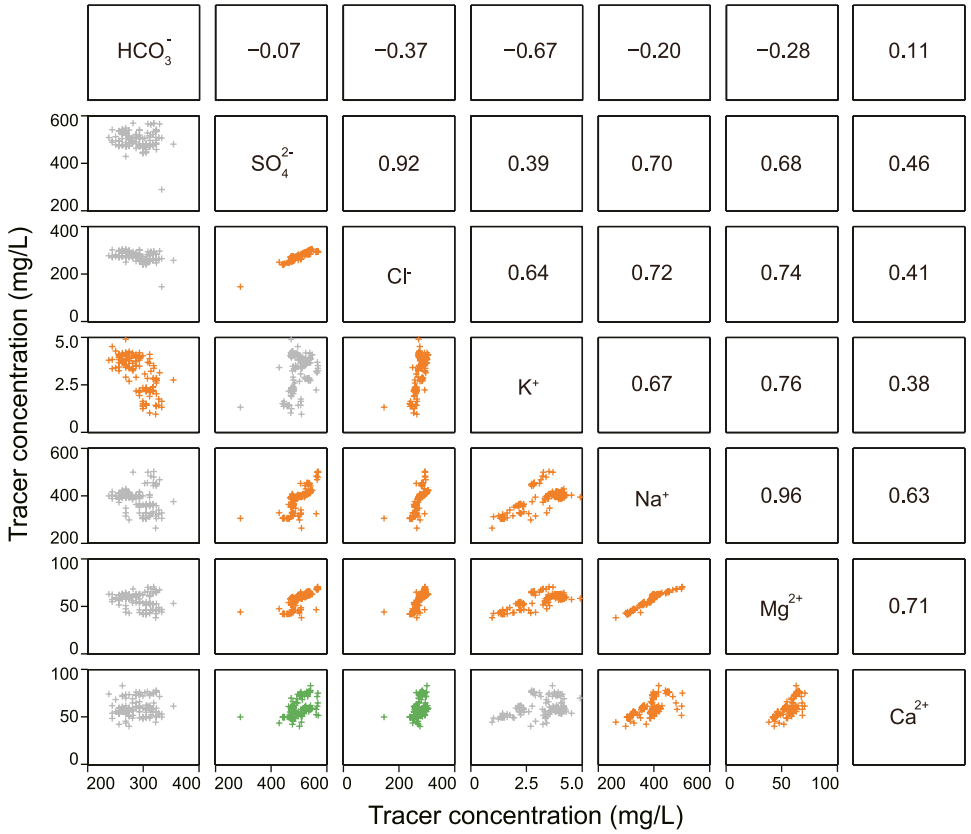

FIGURE 2
Bivariate plots of spring water chemistry at the X10 spring. The top half of the plots represents the Pearson's correlation coefficient (*r*) for the linear relationship between each solute.

primary controlling the evolution of X10 spring and lake water chemistry (Figure 3). The river water (HXG and AKS) is affected by precipitation and rock weathering, which may be related to the geographical features of sampling sites such as elevation, climatic conditions, and tectonic environment. The X10 spring and L1 and L2 lakes, in particular, experience significant evaporation, and the $Na^+/(Na^+ + Ca^{2+})$ ratio of the samples is close to 1, with distribution in the upper right corner (Figure 3A).

To further analyze the water chemistry characteristics and their influencing factors, the time series of major ions in the X10 spring were plotted (Figure 4). The results show that most of the hydrochemical ion concentrations have annual dynamic changes, showing the characteristics of a higher concentration in winter and a lower concentration in summer (Figure 4A). We compared the dynamic water level of the X10 spring with the regional precipitation (precipitation data from The National Oceanic and Atmospheric Administration). Although the annual dynamic variation of the X10 spring water levels is relatively stable, the magnitude and pattern of water level changes are still influenced by precipitation, showing an increase in precipitation followed by a rise in water level. For example, in November 2019, the water level showed a notable upward change of approximately 12 cm, while the precipitation also reached a maximum of 1.2 mm/d concurrently, and the precipitation in winter and spring is markedly higher than that in summer and autumn (Figure 4B). Therefore, there is a large fluctuation in the X10 spring dynamic water level in winter and spring, which is similar to the annual dynamic change of hydrochemical ion concentration. Moreover, the X10 spring (altitude of 1088 m) is located in an area with high topography in the northeast and low topography in the southwest, and the Bogda Mountain (altitude of 5548 m) is located in the east. Its peaks are covered with snow all year round, so it is assumed that the annual dynamic characteristics of hydrochemical components may be affected by the snowmelt in the high mountain area. In addition, we observed notable decreases in hydrochemical ion concentrations (SO_4^{2-}, Cl^-, Na^+, Mg^{2+}, Ca^{2+}, K^+) in the X10 spring, after the Hutubi *M* 4.9 earthquake in Xinjiang on 8 December 2018 (Figure 4A). It took 1–2 months for these parameters to return to normal levels. Notably, HCO_3^- concentrations did not change much before and after the earthquake, and they do not show the characteristic annual change.

4.2 Hydrogen and oxygen stable isotope

The δ^2H and $\delta^{18}O$ values of the X10 spring, rainfall, snowmelt, and surface water are shown in Tables 1, 2. The stable isotope values in the X10 spring were found to range from −13.00‰ to −12.16‰ in $\delta^{18}O$ with an average of −12.46‰ and from −90.6‰ to −87.87‰ in δ^2H with an average of −63.7‰. The isotopic values of surface water varied between −12.01‰ and −9.97‰ in $\delta^{18}O$ with an average of −11.06‰ and from −86.20‰ to −72.08‰ in δ^2H with an average of −76.16‰.

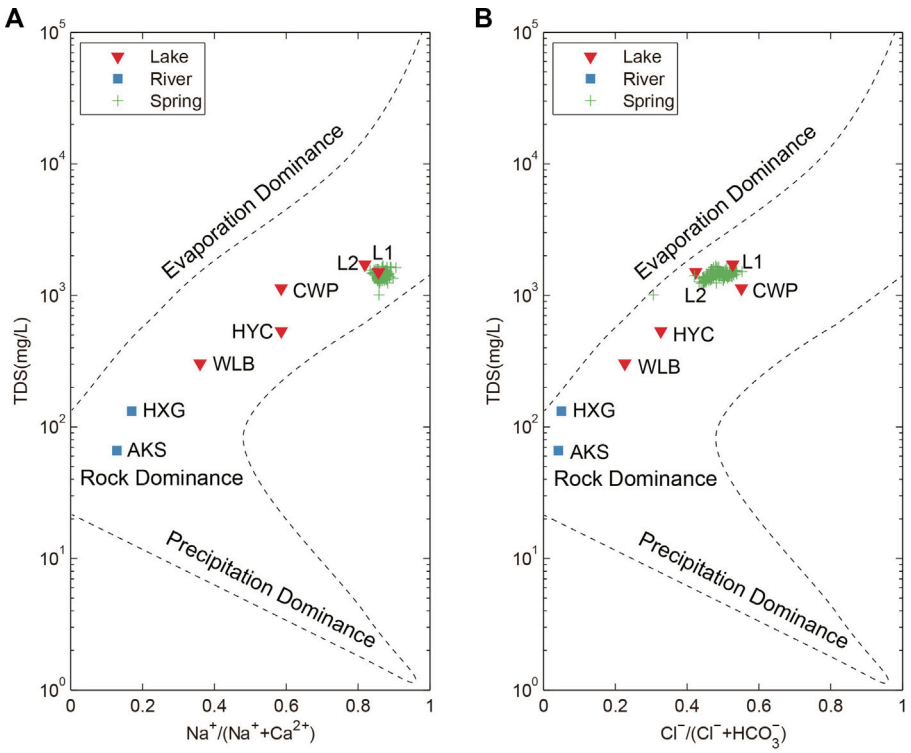

FIGURE 3
Gibbs plots of groundwater and surface water samples in the study area: **(A)** $Na^+/(Na^+ + Ca^{2+})$ and **(B)** $Cl^-/(Cl^- + HCO_3^-)$ *versus* total dissolved solids (TDS).

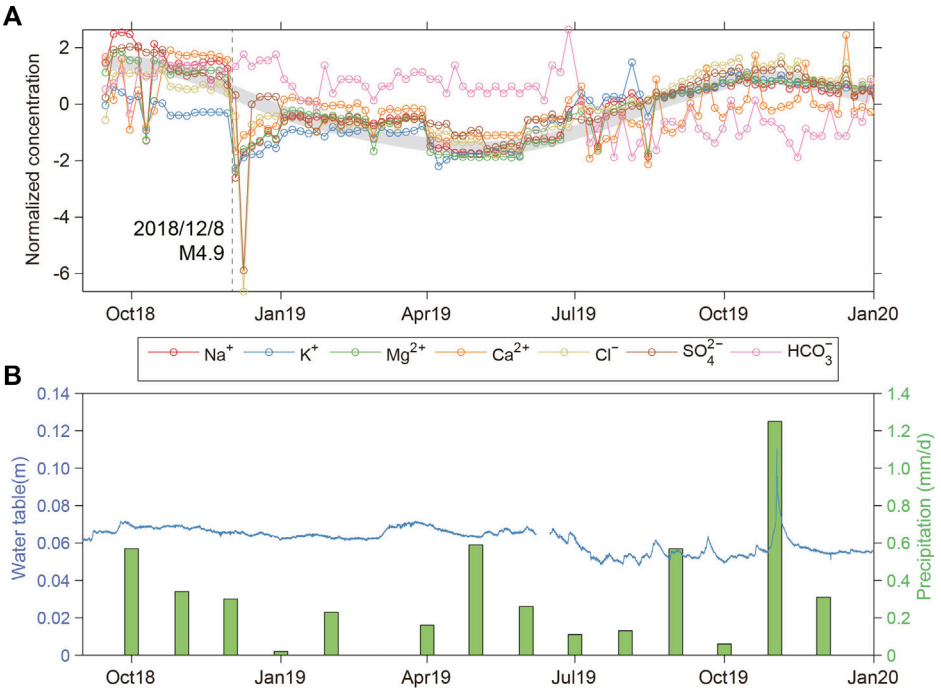

FIGURE 4
Variation of major elements during the study period **(A)** and the comparison diagram of dynamic water level and precipitation in the X10 spring **(B)**. The gray dashed line in **(A)** represents the 8 December 2018, Hutubi *M* 4.9 earthquake in Xinjiang, China.

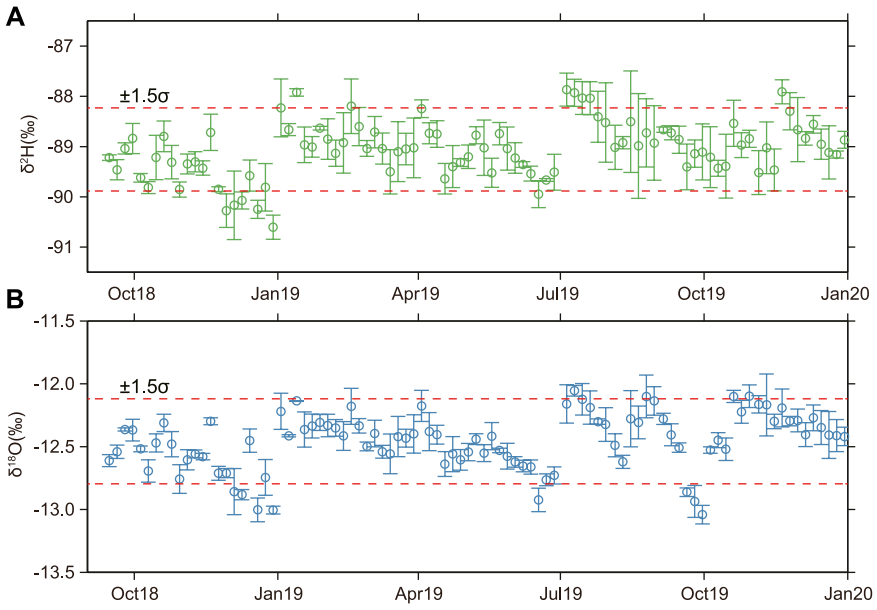

FIGURE 5
Temporal variations in δ^2H **(A)** and $\delta^{18}O$ **(B)** of the X10 spring. The dotted red lines in the figures **(A)** and **(B)** represent the background values expressed as the mean ± 1.5σ. The stable isotope error is assigned to 1σ.

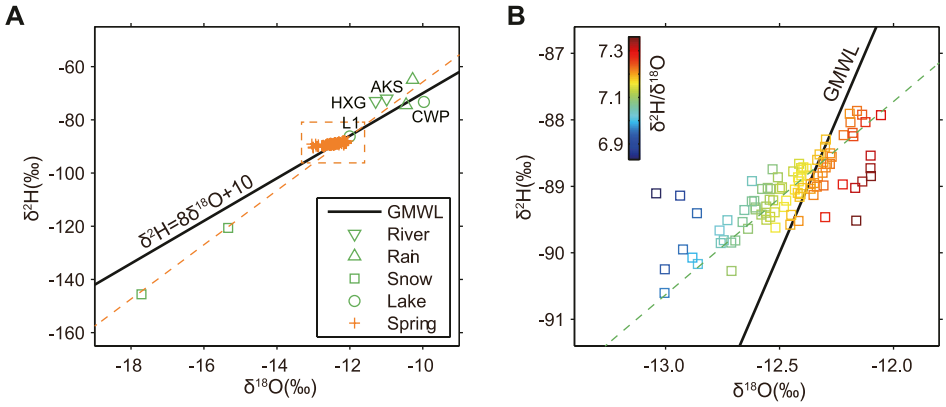

FIGURE 6
The relationship between $\delta^{18}O$ and δ^2H for the samples from different water bodies **(A)** and the enlarged $\delta^{18}O$ and δ^2H time variation in the X10 spring **(B)**.

The variation ranges of δ^2H and $\delta^{18}O$ for rainfall are −74.41‰ to −64.93‰ and −10.46‰ to −10.28‰, respectively, and the variation ranges of δ^2H and $\delta^{18}O$ for snowmelt are −145.59‰ to −120.65‰ and −17.71‰ to −15.34‰, respectively.

Figure 5 shows the time series of changes in hydrogen and oxygen isotopes of the X10 spring. The results show that the overall δ^2H (Figure 5A) and $\delta^{18}O$ (Figure 5B) values are relatively stable without annual variations. The fluctuations are small and mostly within 1.5 times of the variance range, with only individual time values exceeding this range. This is inconsistent with the annual dynamic characteristics exhibited by the hydrochemical ion concentration. All water samples were compared to the Global meteorite water line (GMWL). As shown in Figure 6, most of spring water samples are distributed close to the GMWL and trend line. They are heavier than snowmelt and lighter than rainfall and surface water. This indicates that the X10 spring is derived from meteoric water and is also affected by water–rock interaction and groundwater mixing at different layers. In addition, the hydrogen and oxygen isotope ratio of the X10 spring also deviates from the trend line periodically (Figure 6B), and the $\delta^{18}O$ values show fluctuating changes (increasing or decreasing). This suggests that the hydrogen and oxygen isotopes of the spring may also be influenced by other factors.

5 Discussion

5.1 Analysis of the source of the X10 spring

The chemical composition and isotopes (δ^2H and $\delta^{18}O$) of groundwater are important tools for identifying groundwater recharge sources, determining the degree of water–rock interaction, and tracing the evolution of water chemistry (Craig, 1961; Diaw et al., 2012; Capecchiacci et al., 2015; Pang et al., 2017; Qi et al., 2017). The hydrogen and oxygen isotopic characteristics of global meteoric water show a linear relationship $\delta^2H = 8\delta^{18}O + 10$ (Craig, 1961) that drifts away from the GMWL due to the influence of regional precipitation cycles and recharge sources.

Figure 6A shows that the δ^2H and $\delta^{18}O$ ratios of the X10 spring water, snowmelt, rainfall, and surface water are close to the trend line and GMWL, indicating that they all originated from meteoric water. However, their isotopic characteristics are variable due to the different evaporation, condensation, landing, infiltration, and runoff conditions. The δ^2H and $\delta^{18}O$ ratios of the X10 spring are between snowmelt, rainfall, and surface water (river and lake), The L1 Lake, which is next to the X10 spring, has δ^2H and $\delta^{18}O$ values close to those of the X10 spring, indicating that they are derived from the same recharge. By contrast, the hydrogen and oxygen isotope ratio of the CWP lake, which is farther away from the X10 spring but is close to the AKS and HXG rivers, deviates from the trend line to the right, indicating slight water–rock interaction reflected in ^{18}O exchange, which may result from the interactions of groundwater from deeper layers withe subsurface rocks. This may be related to the geographical location of the CWP lake in the Chaiwobu Basin. It has a low topography, and the northern edge of the basin is the Bogda Mountain (North Mountain), which has a high topography. The AKS and HXG rivers originate from the recharge of snowmelt from the high mountains, and then flow out from the Bogda Pass and recharge the CWP lake after a longer distance. In addition, the δ^2H and $\delta^{18}O$ ratios of the AKS and HXG rivers deviate slightly to the left of the trend line, which can be explained by degassing or by a large deuterium excess related to the climate regime at the time of precipitation. In addition, according to the empirical formula of the relationship between δ^2H, $\delta^{18}O$ and local elevation (Wang, 1991): $\delta^2H = -0.026H - 30.2$, we estimate that the recharge elevation of X10 spring is about 2300 m, and the elevation of the recharge area is higher than the actual elevation of the spring point (1055 m). Therefore, we infer that this spring is supplied by atmospheric precipitation, snowmelt and bedrock fissure water from the Eastern Bogda Mountains. The groundwater infiltrates into the aquifer along the rock fractures, tectonic fractures and pore spaces, thus being transported along channels to the mouth of the spring and finally overflowing at the surface.

The high TDS (mean value of 1.42 g/L) and high concentrations of Na^+, Cl^-, and SO_4^{2-} ions in X10 spring water compared to surface water also reflect the long runoff and deep circulation of groundwater, suggesting that the groundwater circulates to the depth under the action of gravity, and water–rock interaction occurs in contact with surrounding rocks as it moves upward along fault zone and fracture, leading to an increase in dissolved solids. The hydrochemical composition of the X10 spring is the result of the combined effects of water–rock interaction and evaporation (Figure 3). In addition, the annual dynamics variation characteristics of chemical ion concentration in X10 spring may be related to the seasons (temperature) of the region in which it is located or the area of the recharge source, while the time series of hydrogen and oxygen isotopes is relatively stable as a whole (Figure 5), with a small range of variation, indicating that the recharge source and water residence time of the monitored springs are stable. This evidence further supports the stability of the water chemistry in X10 spring. The combined analysis of hydrogen and oxygen stable isotopes and chemical characteristics can more accurately indicate the distance of the recharge source and its recharge relationship with surface water.

5.2 Hydrogeochemical anomalies caused by earthquakes

Variation of ion concentrations in groundwater can record mixing and/or switching between different groundwater sources, water–rock interactions, or some combination of both processes. In general, gradual changes record water–rock interactions or slow mixing of groundwater sources reflecting, such as slow leakage along a fracture, whereas abrupt changes record switching between sources, such as a sudden rupture of a hydrological barrier between sources (Skelton et al., 2019). In seismically active regions, tectonic activity may lead to structural changes in the permeability of aquifers and surrounding rocks, such as enhancing water–rock interaction between groundwater and surrounding rocks and accelerating mixing between groundwater from different sources (Tsunogai and Wakita, 1995; Wasteby et al., 2014; Andrén et al., 2016), which cause hydrogeochemical changes to occur rapidly (Thomas, 1988; Claesson et al., 2007). Studies have shown that earthquakes closer to the epicenter or with larger magnitudes may cause hydrogeochemical anomalies (Claesson et al., 2004; Skelton et al., 2014; Onda et al., 2018), and seismic energy density can be used to assess hydrological phenomena associated with earthquakes (Wang, 2007; Wang and Manga, 2010). We analyzed hydrochemical parameters and hydrogen and oxygen stable isotope time series (Supplementary Figure S1 and Figure 7), and earthquakes (Supplementary Table S1) during the study period. The hydrogeochemical characteristics of X10 springs are stable, this invariability is proven by low values of the coefficient of variation (<0.33), which is the ratio between the standard deviation (σ) and the absolute value of the mean ($|\mu|$) of data reported in Supplementary Table S2. Therefore, the possible anomalies connected with transient phenomena like earthquakes could be easily identifiable (Barberio et al., 2017).

A comparison analysis, along with the results shown in Figure 6, was conducted on the monthly cumulative seismic energy density with the time series of hydrogen and oxygen isotope ratio and HCO_3^- concentrations of earthquakes of intensity M 3 or above occurring within 150 km of the X10 spring (Figure 7). Although the hydrogen and oxygen isotope ratios of the X10 spring were generally close to the GMWL and trend line (Figure 6A), there were deviations from the data. Some δ^2H and $\delta^{18}O$ ratios were higher or lower (Figure 6B). The changes in δ^2H and $\delta^{18}O$ ratios and HCO_3^- concentration were relatively consistent, and they showed a negative correlation (Figure 7). The δ^2H and $\delta^{18}O$ ratios change significantly when the surrounding small seismicity activity intensifies. For example, the δ^2H and $\delta^{18}O$ ratios show different degrees of changes (gray bars) during the five time periods of October–December 2018, May–June, July–August, September–October and November–December 2019, with the most significant changes during July–August,

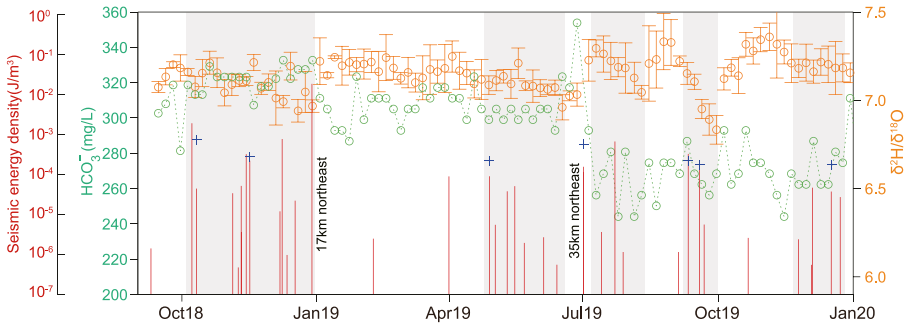

FIGURE 7
Comparison of hydrogen and oxygen isotope ratios, HCO_3^- concentration, and seismic activity during the study period. The red vertical line represents the cumulative seismic energy density, and the yellow and green circles indicate the hydrogen and oxygen isotope ratio and the HCO_3^- concentration, respectively.

September–October and November–December 2019. In the low seismicity case, the hydrogen and oxygen isotope ratio increases gradually, and the value is relatively high. While in the high seismicity case, it gradually decreases. The decrease in hydrogen and oxygen isotopes in May–June 2019 does not change significantly and is only slightly lower than the value before the decrease (low seismic activity), which may be related to the regional cumulative seismic energy density, which is lower during this period. Also, during the high seismic activity in October–December 2018, the hydrogen and oxygen isotope ratio showed a significant fluctuating change, unlike its steady change, during the low seismic activity (January–April 2019). We believe that whether it is a decreasing change or fluctuating change in hydrogen and oxygen isotopes, the above phenomena indicate that the X10 spring recharge water source changed during the period of enhanced seismic activity, showing that the hydrogen and oxygen isotope ratios are more sensitive to small seismic activity. The observed strain data show that the areal strain near the X10 spring has been continuously increasing since September 2018, especially after April 2019 (Supplementary Figure S1), it reflects that the longer the regional stress loading time, the greater the stress accumulation, the more obvious the change of rock deformation or fracture state of the subsurface medium caused by local tectonic activity (i.e., seismic activity), which continuously changes the permeability structure of the fault zone or aquifer (Reddy and Nagabhushanam, 2012; Skelton et al., 2019; Hosono et al., 2020), so that the mixing ratio of the X10 spring recharge source constantly changes, causing deviations in the hydrogen-oxygen isotope ratio. When the recharge source is stable or the mixing ratio of groundwater from different aquifers is very small, the major ion concentration hardly changes. This phenomenon has been confirmed by previous studies (Skelton et al., 2014).

In case of a single earthquake, especially near to the X10 spring or occurring in the eastern recharge source region (N43.62°–N43.83°, E87.85°–E88.02°). For example, the 28 December 2018 Shayba *M*4.3 earthquake (epicenter distance of 17 km), and the 1 July 2019 Midong *M*3.5 earthquake (epicenter distance of 35 km), we observed a decrease in HCO_3^- concentration and an increase in the hydrogen and oxygen isotope ratio, and this suggests an alteration in the recharge source and water-rock interaction of the X10 spring. The seismic energy density of the two earthquakes is 1.66×10^{-2} J/m^3 (*M*4.3) and 1.46×10^{-4} J/m^3 (*M*3.5), respectively, among which the *M*4.3 earthquake in Shayba has the largest seismic energy density (Supplementary Table S1). This confirms the larger isotopic anomaly variation when e > 10^{-4} J/m^3 (Skelton et al., 2014), indicating that the range of isotopic variation may be affected by the earthquake magnitude and distance from the epicenter. However, there are exceptions, for example, after the 8 December 2018 Hutubi M4.9 earthquake in Xinjiang (epicenter distance of 98 km), we observed dramatic decreasing changes in SO_4^{2-}, Cl^-, Na^+, Mg^{2+}, Ca^{2+}, and K^+ concentrations. In addition, there is no change in hydrogen and oxygen isotope ratio and HCO_3^- concentration (Figure 4), and the seismic energy density of this earthquake is 7.12×10^{-4} J/m3. We believe that the decrease in hydrochemical ion concentration after the earthquake can be explained by the decrease in permeability of the fault zone and aquifer caused by the earthquake (Wästeby et al., 2014; Chen and Wang, 2021), showing that the X10 spring recharge source does not change or the proportion of groundwater recharge from deeper parts is small enough to cause isotopic changes in the spring. In addition, for the 7 October 2018 Urumqi *M*4.7 earthquake, concentration variations in individual ions are also observed, but their changes are small, while there are no changes in hydrochemical ion concentrations and stable isotopes in the 22 July 2019 Xinjiang Heshuo M5.0 earthquake, so they are not discussed in this study. We calculated the limited observation data of X10 spring (Supplementary Table S1), and obtained some preliminary understanding that when the earthquake magnitude is greater than *M*4.5 and the epicenter distance is less than 100 km, it can cause changes in the concentrations of major chemical ions in the monitored spring, and when the earthquake magnitude is greater than *M*3.5 and the epicenter distance is less than 50 km, the HCO_3^-concentration and hydroxide isotope will change simultaneously.

Previous studies on seismicity (moderate or large earthquakes above *M*5) and hydrochemical parameter changes in hot springs have been widely reported (Skelton et al., 2014; Skelton et al., 2019, Zhang et al., 2020). They suggested that hot springs are a surface display of geothermal energy in the inside of the Earth, providing insight into thermal transport and water-rock interactions in deep subsurface hot water flow (circulating at depths of up to several thousand kilometers), which can help capturing earthquake precursor information related to

tectonic activities. This study differs from the previous works in that the X10 spring is a cold-water spring (spring temperature about 11.4°C), and its groundwater circulation depth may be shallow in comparison with the hot springs, or it may be derived mainly from the mixing of shallow groundwater. However, due to its particular tectonic location which is situated at the intersection of fault zones, the stress tends to concentrate, which makes the monitoring spring to be sensitive to stress/strain response, thus the spring chemical parameters can easily show the influence on the earthquake. Also, it shows that the fault zone plays an important role in controlling the regional groundwater flow and circulation. Hydrogen and oxygen isotope changes should be taken into account in groundwater resource utilization and management and earthquake precursor monitoring in seismically active areas.

The mechanism of the abovementioned permeability change is only for the limited observation data in this study. A more reasonable mechanism requires more data accumulation. The mechanism by which permeability changes occur in any particular case remains uncertain, and in a natural situation it may be impossible to determine due to the complexity and inaccessibility of the subsurface (Manga et al., 2012). Few studies have been conducted to determine the mechanism between earthquakes and hydrogeochemical changes in cold spring. However, this is important for us to explore the coupling between earthquakes and hydrochemical parameters so that we can have a good insight into earthquakes precursors and post–earthquake healing processes in faults or aquifers (Ingebritsen and Manga, 2014). We also expect to accumulate more similar results in the future by increasing the measurement frequency of hydrochemistry samples in X10 spring, or by conducting water level observation with a higher sampling rate (seconds) or some other observations in more measurement points (De Luca et al., 2018), it would help to test some of the proposed mechanisms and identify the controls on permeability and its evolution.

6 Conclusion

Based on continuous monitoring data of chemical composition and hydrogen and oxygen stable isotopes of the X10 spring in Xinjiang, China, we analyzed its recharge source and water chemical evolution. The correlation between hydrogeochemical changes and seismicity is discussed by comparing with local earthquakes and mechanism of changes are explained. The following results can be inferred: 1) the chemical type of the X10 spring water is SO_4·Cl–Na, which belongs to the medium mineralization water. The average value of TDS is 1.42 g/L. The dominant cations are Na^+ and Ca^{2+}, and the dominant anions are SO_4^{2-} and HCO_3^-. Na^+ and Mg^{2+}, and SO_4^{2-} and Cl^-have the strongest correlation, and HCO_3^- is not affected by other ions. 2) The δ^2H of the X10 spring varies from −90.60‰ to 87.87‰, with an average value of −89.06‰ and $\delta^{18}O$ varies from −13.00‰ to −12.16‰, with an average value of −12.46‰. This is mainly distributed along the global meteoric water line and trend line, indicating that the spring originates from long-distant meteoric water, snowmelt, and bedrock fissure water in high mountainous areas. 3) The chemical components of the X10 spring are affected by water–rock interaction and evaporation, and most of the ion concentrations, except HCO_3^-, have an annual dynamic pattern, showing high in winter and low in summer, related to the seasonal effect of snowmelt. 4) The hydrochemistry changes near the epicenter are attributed to changes in the permeability of the fault zone or aquifer caused by tectonic activity. The hydrogen and oxygen stable isotopes and HCO_3^- concentrations are sensitive to local small seismic activities.

Data availability statement

The original contributions presented in the study are included in the article/Supplementary Material, further inquiries can be directed to the corresponding author.

Author contributions

YX and SP wrote the manuscript.

Funding

This research was supported by the National Natural Science Foundation of China (41972253), Green, Intelligent and Safe Mining for Coal Resources (52121003).

Acknowledgments

We thank the Earthquake Agency of Xinjiang Uygur Autonomous Region for providing the data for this study. The information on the earthquakes was obtained from the website of CEIC (https://news.ceic.ac.cn). We also thank the editor and other reviewers for their positive and helpful comments on our manuscript.

Conflict of interest

The authors declare that the research was conducted in the absence of any commercial or financial relationships that could be construed as a potential conflict of interest.

Publisher's note

Supplementary material

The Supplementary Material for this article can be found online at: https://www.frontiersin.org/articles/10.3389/feart.2022.1100068/full#supplementary-material

References

Andrén, M., Stockmann, G., Skelton, A., Sturkell, E., Mörth, C. M., Guðrúnardóttir, H. R., et al. (2016). Coupling between mineral reactions, chemical changes in groundwater, and earthquakes in Iceland. *J. Geophys. Res. Solid Earth* 121, 2315–2337. doi:10.1002/2015JB012614

Barberio, M. D., Barbieri, M., Billi, A., Doglioni, C., and Petitta, M. (2017). Hydrogeochemical changes before and during the 2016 amatrice-norcia seismic sequence (central Italy). *Sci. Rep.* 7 (11735), 11735. doi:10.1038/s41598-017-11990-8

Capecchiacci, F., Tassi, F., Vaselli, O., Bicocchi, G., Gabassi, J., Giannini, I., et al. (2015). A combined geochemical and isotopic study of the fluids discharged from the Montecatini thermal system (NW Tuscany, Italy). *Appl. Geochem.* 59, 33–46. doi:10.1016/j.apgeochem.2015.03.010

Chen, L., and Wang, G. (2021). Hydrochemical changes of a spring due to the may 30, 2014 *Ms* 6.1 yingjiang earthquake, southwest China. *Environ. Pollut.* 284 (4), 117125. doi:10.1016/j.envpol.2021.117125

Claesson, L., Skelton, A., Graham, C., Dietl, C., Mörth, C.-M., Torssander, P., et al. (2004). Hydrogeochemical changes before and after a major earthquake. *Geology* 32, 641–644. doi:10.1130/g20542.1

Claesson, L., Skelton, A., Graham, C., and Mörth, C.-M. (2007). The timescale and mechanisms of fault sealing and water-rock interaction after an earthquake. *Geofluids* 7, 427–440. doi:10.1111/j.1468-8123.2007.00197.x

Cortes, J. E., Muñoz, L. F., Gonzalez, C. A., Niño, J. E., Polo, A., Suspes, A., et al. (2016). Hydrogeochemistry of the formation waters in the San Francisco field, UMV basin, Colombia – a multivariate statistical approach. *J. Hydrol.* 539, 113–124. doi:10.1016/j.jhydrol.2016.05.010

Craig, H. (1961). Isotopic variations in meteoric waters. *Science* 133 (3465), 1702–1703. doi:10.1126/science.133.3465.1702

Dadomo, A., Lemmi, M., Martinelli, G., Menichetti, M., and Telesca, L. (2013). Springwater continuous monitoring in the l'aquila area in concomitance with the april 2009 seismic swarm in central Italy: Constraining factors to possible deep-seated fluid emissions. *Chem. Geol.* 339, 169–176. doi:10.1016/j.chemgeo.2012.07.011

De Luca, G., Di Carlo, G., and Tallini, M. (2018). A record of changes in the Gran Sasso groundwater before, during and after the 2016 Amatrice earthquake, central Italy. *Sci. Rep.* 8, 15982. doi:10.1038/s41598-018-34444-1

Diaw, M., Faye, S., Stichler, W., and Maloszewski, P. (2012). Isotopic and geochemical characteristics of groundwater in the Senegal river delta aquifer: Implication of recharge and flow regime. *Environ. Earth Sci.* 66 (4), 1011–1020. doi:10.1007/s12665-010-0710-4

Du, J., Si, X., Chen, Y., Fu, H., Jian, C., and Guo, W. (2008). *Geochemical anomalies connected with great earthquakes in China, Geochemistry Research Advances*. New York: Nova Science Publishers Inc, 57–92.

Du, J., Amita, K., Ohsawa, S., Zhang, Y., Kang, C., and Yamada, M. (2010). Experimental evidence on formation of imminent and short-term hydrochemical precursors for earthquakes. *Appl. Geochem.* 25 (4), 586–592. doi:10.1016/j.apgeochem.2010.01.015

Elkhoury, J. E., Brodsky, E. E., and Agnew, D. C. (2006). Seismic waves increase permeability. *Nature* 441, 1135–1138. doi:10.1038/nature04798

Etiope, G., Calcara, M., and Quattrocchi, F. (1997). Seismogeochemical algorithms for earthquake prediction: an overview. *Ann. Geophys.* 40 (6). doi:10.4401/ag-3825

Gibbs, R. J. (1970). Mechanisms controlling world water chemistry. *Science* 170 (3962), 1088–1090. doi:10.1126/science.170.3962.1088

Hosono, T., and Masaki, Y. (2020). Post-seismic hydrochemical changes in regional groundwater flow systems in response to the 2016 *Mw* 7.0 Kumamoto earthquake. *J. Hydrol.* 580, 124340. doi:10.1016/j.jhydrol.2019.124340

Hosono, T., Yamada, C., Manga, M., Wang, C. Y., and Tanimizu, M. (2020). Stable isotopes show that earthquakes enhance permeability and release water from mountains. *Nat. Commun.* 11, 2776. doi:10.1038/s41467-020-16604-y

Inan, S., Balderer, W., Leuenberger, F., Yakan, H., Özvan, Ali., and Freund, F. T. (2013). Springwater chemical anomalies prior to the *Mw* = 7.2 van earthquake (Turkey). *Geochem. J.* 46 (1), E11–E16. doi:10.2343/geochemj.1.0159

Ingebritsen, S. E., and Manga, M. (2014). Hydrogeochemical precursors. *Nat. Geosci.* 7 (10), 697–698. doi:10.1038/ngeo2261

Kim, J., Lee, J., Petitta, M., Kim, H., Kaown, D., Park, I. W., et al. (2019). Groundwater system responses to the 2016 M_L 5.8 Gyeongju earthquake, South Korea. *J. Hydrol.* 576, 150–163. doi:10.1016/j.jhydrol.2019.06.044

Kim, J., Joun, W.-T., Lee, S., Kaown, D., and Lee, K.-K. (2020). Hydrogeochemical evidence of earthquake–induced anomalies in response to the 2017 M_W 5.5 Pohang earthquake in Korea. *Geochem. Geophys. Geosyst.* 21, e2020GC009532. doi:10.1029/2020GC009532

King, C.-Y., Koizumi, N., and Kitagawa, Y. (1995). Hydrogeochemical anomalies and the 1995 kobe earthquake. *Science* 269, 38–39. doi:10.1126/science.269.5220.38

King, C.-Y. (2018). Characteristics of a sensitive well showing pre-earthquake water-level changes. *Pure Appl. Geophys.* 175, 2411–2424. doi:10.1007/s00024-018-1855-4

Li, B., Shi, Z., Wang, G., and Liu, C. (2019). Earthquake-related hydrochemical changes in thermal springs in the Xianshuihe Fault zone, Western China. *J. Hydrol.* 579, 124175. doi:10.1016/j.jhydrol.2019.124175

Manga, M., and Wang, C. Y. (2015). "Earthquake hydrology," in *Treatise on Geophysics*. Second Edition (Elsevier), 4, 305–328.

Manga, M., Beresnev, I., Brodsky, E. E., Elkhoury, J. E., Elsworth, D., and Ingebritsen, S. E. (2012). Changes in permeability caused by transient stresses: Field observations, experiments, and mechanisms. *Reviews of Geophysics* 50 (2)

Mastrorillo, L., Saroli, M., Viaroli, S., Banzato, F., Valigi, D., and Petitta, M. (2020). Sustained post-seismic effects on groundwater flow in fractured carbonate aquifers in Central Italy. *Hydrol. Process* 34, 1167–1181. doi:10.1002/hyp.13662

Mohr, C. H., Manga, M., Wang, C.-Y., and Korup, O. (2017). Regional changes in streamflow after a megathrust earthquake. *Earth Planet. Sci. Lett.* 458, 418–428. doi:10.1016/j.epsl.2016.11.013

Onda, S., Sano, Y., Takahata, N., Kagoshima, T., Miyajima, T., Shibata, T., et al. (2018). Groundwater oxygen isotope anomaly before the *M*6.6 Tottori earthquake in Southwest Japan. *Sci. Rep.* 8, 4800. doi:10.1038/s41598-018-23303-8

Pang, Z. H., Kong, Y. L., Li, J., and Tian, J. (2017). An isotopic geoindicator in the hydrological cycle. *Procedia Earth Planet. Sci.* 17, 534–537. doi:10.1016/j.proeps.2016.12.135

Qi, J. H., Xu, M., An, C. J., Wu, M. L., Zhang, Y. H., Li, X., et al. (2017). Characterizations of geothermal springs along the Moxi deep fault in the Western Sichuan plateau, China. *Phys. Earth Planet Inter.* 263, 12–22. doi:10.1016/j.pepi.2017.01.001

Reddy, D. V., and Nagabhushanam, P. (2012). Chemical and isotopic seismic precursory signatures in deep groundwater: Cause and effect. *App. Geochem.* 27, 2348–2355. doi:10.1016/j.apgeochem.2012.08.023

Reddy, D. V., Nagabhushanam, P., and Sukhija, B. S. (2011). Earthquake (*M* 5.1) induced hydrogeochemical and $\delta^{18}O$ changes: validation of aquifer breaching—mixing model in koyna, India. *Geophys. J. Int.* 184 (1), 359–370. doi:10.1111/j.1365-246x.2010.04838.x

Rosen, M. R., Binda, G., Archer, C., Pozzi, A., Michetti, A. M., and Noble, P. J. (2018). Mechanisms of earthquake-induced chemical and fluid transport to carbonate groundwater springs after earthquakes. *Water Resour. Res.* 54, 5225–5244. doi:10.1029/2017wr022097

Shi, Z., Wang, G., and Liu, C. (2017). Co-seismic groundwater level changes induced by the may 12, 2008 wenchuan earthquake in the near field. *Pure Appl. Geophys* 170 (11), 1773–1783. doi:10.1007/s00024-012-0606-1

Shi, Z., Wang, G., Wang, C. Y., Manga, M., and Liu, C. (2014). Comparison of hydrological responses to the wenchuan and lushan earthquakes. *Earth Planet. Sci. Lett.* 391, 193–200. doi:10.1016/j.epsl.2014.01.048

Shi, Z., Zhang, H., and Wang, G. (2020). Groundwater trace elements change induced by M 5.0 earthquake in Yunnan. *J. Hydrol.* 581, 124424. doi:10.1016/j.jhydrol.2019.124424

Skelton, A., Claesson, L., Chakrapani, G., Mahanta, C., Routh, J., Mörth, M., et al. (2008). Coupling between seismic activity and hydrogeochemistry at the shillong plateau, northeastern India. *Pure Appl. Geophys.* 165, 45–61. doi:10.1007/s00024-007-0288-2

Skelton, A., Andrén, M., Kristmannsdóttir, H., Stockmann, G., Mörth, C. M., Sveinbjörnsdóttir, Á., et al. (2014). Changes in groundwater chemistry before two consecutive earthquakes in Iceland. *Nat. Geosci.* 7 (10), 752–756. doi:10.1038/ngeo2250

Skelton, A., Liljedahl-Claesson, L., Wästeby, N., Andrén, M., Stockmann, G., Sturkell, E., et al. (2019). Hydrochemical changes before and after earthquakes based on long-term measurements of multiple parameters at two sites in northern Iceland—a review. *J. Geophys. Res. Solid Earth* 124 (3), 2702–2720. doi:10.1029/2018JB016757

Song, S. R., Chen, Y. L., Liu, C. M., Ku, W. Y., Chen, H. F., Liu, Y. J., et al. (2005). Hydrochemical changes in spring waters in taiwan: Implications for evaluating sites for earthquake precursory monitoring. *Tao. Terr. Atmos. Ocean. Sci.* 16 (4), 745. doi:10.3319/tao.2005.16.4.745(gig)

Sun, X., Xiang, Y., and Shi, Z. (2018a). Estimating the hydraulic parameters of a confined aquifer based on the response of groundwater levels to seismic Rayleigh waves. *Geophys. J. Int.* 213 (2), 919–930. doi:10.1093/gji/ggy036

Sun, X., Xiang, Y., Shi, Z., and Wang, B. (2018b). Preseismic changes of water temperature in the yushu well, Western China. *Pure Appl. Geophys.* 175, 2445–2458. doi:10.1007/s00024-017-1579-x

Thomas, D. (1988). Geochemical precursors to seismic activity. *Pure Appl. Geophys.* 126 (2), 241–266. doi:10.1007/bf00878998

Tsunogai, U., and Wakita, H. (1995). Precursory chemical changes in ground water: Kobe earthquake, Japan. *Science* 269 (5220), 61–63. doi:10.1126/science.269.5220.61

Wakita, H. (1975). Water wells as possible indicators of tectonic strain. *Science* 189 (4202), 553–555. doi:10.1126/science.189.4202.553

Wakita, H. (1996). Geochemical challenge to earthquake prediction. *PNAS* 93 (9), 3781–3786. doi:10.1073/pnas.93.9.3781

Wang, C. Y., and Manga, M. (2010). "Earthquakes and water," in *Lecture notes in Earth sciences*, (Berlin: Springer) 249.

Wang, C. Y., and Manga, M. (2015). New streams and springs after the 2014 M_w6.0 south napa earthquake. *Nat. Commun.* 6, 7597. doi:10.1038/ncomms8597

Wang, R., Woith, H., Milkereit, C., and Zschau, J. (2004). Modelling of hydrogeochemical anomalies induced by distant earthquakes. *Geophys. J. Int.* 157 (2), 717–726. doi:10.1111/j.1365-246x.2004.02240.x

Wang, C. H., Wang, C. Y., Kuo, C. H., and Chen, W. F. (2005). Some isotopic and hydrological changes associated with the 1999 Chi-Chi earthquake, Taiwan. *Isl. Arc* 14 (1), 37–54. doi:10.1111/j.1440-1738.2004.00456.x

Wang, H. (1991). Introduction to Isotope Hydrogeology. Beijing: Geological Publishing House. (in Chinese).

Wang, C. Y. (2007). Liquefaction beyond the near field. *Seismol. Res. Lett.* 78 (5), 512–517. doi:10.1785/gssrl.78.5.512

Wästeby, N., Skelton, A., Tollefsen, E., Andrén, M., Stockmann, G., Claesson-Liljedahl, L., et al. (2014). Hydrochemical monitoring, petrological observation, and geochemical modeling of fault healing after an earthquake: *J. Geophys. Res. Solid Earth* 119 (7), 5727–5740. doi:10.1002/2013JB010715

Woith, H., Wang, R., Maiwald, U., Pekdeger, A., and Zschau, J. (2013). On the origin of geochemical anomalies in groundwaters induced by the Adana 1998 earthquake. *Chem. Geol.* 339 (2), 177–186. doi:10.1016/j.chemgeo.2012.10.012

Yang, P., Sun, X., Liu, D. Y., He, Z., and Li, Y. (2021). Hydrochemical characteristics of groundwater at the epicenter of the 2021 biru *M*6.1 earthquake in central tibet. *Water* 13, 3111. doi:10.3390/w13213111

Zhang, L., Guo, L., Wang, Y., Liu, D., and Li, J. (2020). Continuous monitoring of hydrogen and oxygen stable isotopes in a hot spring: significance for distant earthquakes. *Applied Geochemistry* 112, 104488. doi:10.1016/j.apgeochem.2019.104488